EDGE ARTICLE

Conformation control through concurrent N–H⋯S and N–H⋯O=C hydrogen bonding and hyperconjugation effects†

Zeynab Imani, ‡[a] Venkateswara Rao Mundlapati, ‡[b] Gildas Goldsztejn, §[b] Valérie Brenner, [b] Eric Gloaguen, [b] Régis Guillot, [a] Jean-Pierre Baltaze, [a] Katia Le Barbu-Debus, [c] Sylvie Robin, [ad] Anne Zehnacker, [c] Michel Mons *[b] and David J. Aitken *[a]

In addition to the classical N–H⋯O=C non-covalent interaction, less conventional types of hydrogen bonding, such as N–H⋯S, may play a key role in determining the molecular structure. In this work, using theoretical calculations in combination with spectroscopic analysis in both gas phase and solution phase, we demonstrate that both these H-bonding modes exist simultaneously in low-energy conformers of capped derivatives of Attc, a thietane α-amino acid. 6-Membered ring inter-residue N–H⋯S interactions ($C6^\gamma$), assisted by hyperconjugation between the thietane ring and the backbone, combine with 5-membered ring intra-residue backbone N–H⋯O=C interactions (C5) to provide a $C5$–$C6^\gamma$ feature that stabilizes a planar geometry in the monomer unit. Two contiguous $C5$–$C6^\gamma$ features in the planar dimer implicate an unprecedented three-centre H-bond of the type C=O⋯H(N)⋯SR$_2$, while the trimer adopts two $C5$–$C6^\gamma$ features separated by a Ramachandran α-type backbone configuration. These low-energy conformers are fully characterized in the gas phase and support is presented for their existence in solution state.

Introduction

The hydrogen bond (H-bond) plays a supremely important role in determining the structure and the behaviour of countless molecules of all sizes.[1] Chemists have harnessed hydrogen bonding as a tool, with applications ranging from selective synthesis,[2] to crystal engineering[3,4] to the design of self-organizing molecular and supramolecular architectures.[5,6] Nature makes use of hydrogen bonding, along with other types of non-covalent interactions, to define and control not only the shapes of biomolecules but also the specific interactions between them.[7–9] The most commonly observed (and the best studied) type of H-bond in proteins is the N–H⋯O=C interaction between backbone amide functions, which stabilizes the familiar regular secondary structures of helices and sheets, as well as β-turns and γ-turns which are formed by cyclic 10-membered ring (C10) or cyclic 7-membered ring (C7) H-bonds (Fig. 1).[10–12] Recently, there has been an increased awareness of the importance of contributions to secondary structure stabilization from other types of non-covalent interactions, including less conventional H-bonds such as intra-residue C5 H-bonds (Fig. 1),[13–15] or C–H⋯O interactions,[16,17] as well as phenomena such as $n \rightarrow \pi^*$ hyperconjugative interactions,[18] C-bonds,[19] cation–π interactions,[20,21] and others.[22]

Reports of non-covalent interactions in proteins which specifically implicate the side-chain heteroatom of sulfur-containing residues are rare and do not involve H-bonds; rather, they take the form of sulfur–aromatic interactions[23,24] or chalcogen bonds.[25] Studies on small peptide systems have revealed that backbone–backbone H-bonding interactions may exist in thioamides.[26,27] Nonetheless, it was generally assumed for some time that a side-chain thioether was a poor H-bond acceptor and that N–H⋯S interactions between amide backbones and the sulfur atom of methionine were weak and of little significance.[28,29]

Recent observations on model systems have challenged this credo, however. Gas phase spectroscopic studies supported by quantum calculations suggested a significant role for short-range $C7^\delta$ inter-residue and $C6^\delta$ intra-residue N–H⋯S interactions, implicating the sulfur in the δ-position of the side chain,

[a]Institut de Chimie Moléculaire et des Matériaux d'Orsay (ICMMO), CNRS, Université Paris-Saclay, 91405 Orsay, France. E-mail: david.aitken@u-psud.fr

[b]Laboratoire Interactions, Dynamiques et Lasers (LIDYL), CEA, CNRS, Université Paris-Saclay, 91191 Gif-sur-Yvette, France. E-mail: michel.mons@cea.fr

[c]Institut des Sciences Moléculaires d'Orsay (ISMO), CNRS, Université Paris-Saclay, 91405 Orsay, France

[d]Faculté de Pharmacie, Université de Paris, 75006 Paris, France

† Electronic supplementary information (ESI) available. CCDC 1985233–1985235. For ESI and crystallographic data in CIF or other electronic format see DOI: 10.1039/d0sc03339a

‡ These authors contributed equally to this work.

§ Current address: ISMO, CNRS, Université Paris-Saclay, 91405 Orsay, France.
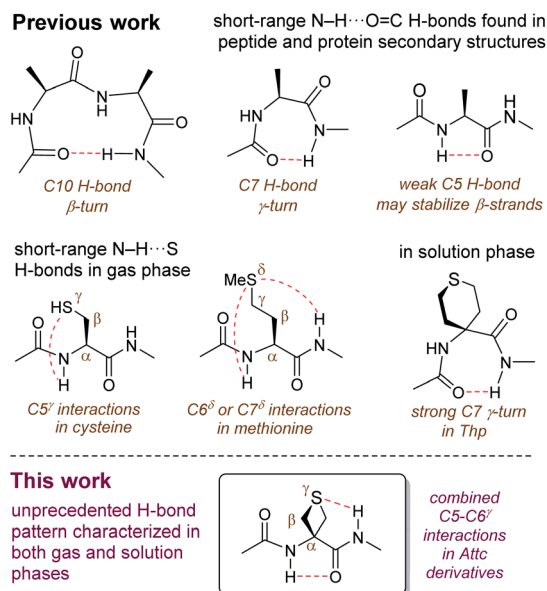
Previous work

short-range N–H···O=C H-bonds found in peptide and protein secondary structures

C10 H-bond
β-turn

C7 H-bond
γ-turn

weak C5 H-bond
may stabilize β-strands

short-range N–H···S
H-bonds in gas phase

in solution phase

C5$^\gamma$ interactions
in cysteine

C6$^\delta$ or C7$^\delta$ interactions
in methionine

strong C7 γ-turn
in Thp

This work
unprecedented H-bond pattern characterized in both gas and solution phases

combined
C5-C6$^\gamma$
interactions
in Attc
derivatives

Fig. 1   Background for this study.

in derivatives of methionine (Fig. 1).[30] An assessment of the strength of these H-bonds found them to be comparable with those of classical N–H···O=C interactions.[31] Related studies showed that C5$^\gamma$ intra-residue N–H···S H-bonds, implicating the sulfur in the γ-position, may contribute to the non-covalent interactions on the conformational landscape of cysteine derivatives in the gas phase (Fig. 1).[32,33] Solution state evidence for such interactions has been scarce. C5 and C6 H-bond interactions implicating sulfur have been suggested in non-peptide arylthioether oligomers.[34,35] In early work on peptides, it was suggested that intra-residue C5$^\gamma$ N–H···S interactions may exist in short oligomers of *S*-methylcysteine,[36] although this had no apparent impact on secondary structure, since the appearance of helical conformations was indicated for oligomers longer than the pentamer.[37] Likewise, short oligomers of methionine (smaller than the hexamer) do not show any conformational preferences,[38] while short peptide derivatives of 4-aminotetrahydrothiopyran-4-carboxylic acid (Thp) adopt standard C7 (or C10) conformers (Fig. 1) with no apparent role for sulfur.[39,40]

In order to probe the potential of short-range N–H···S interactions with a view to controlling model peptide edifices we examined derivatives of 3-aminothietane-3-carboxylic acid (Attc)
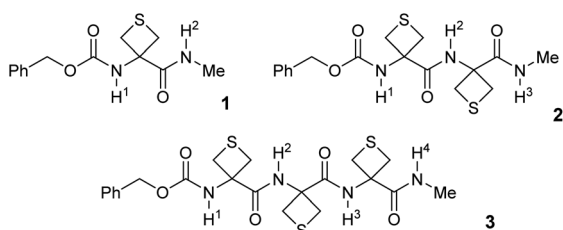

Fig. 2   Structures of the compounds 1–3 used in this study.

(Fig. 2). In principle, we felt that Attc might support C5 or C6$^\gamma$ N–H···S interactions, although the geometrical constraints imposed by the 4-membered ring might result in a bias for one or other of these features. In the event, we have discovered that short oligomers of this α-amino acid (up to a trimer) adopt a previously unknown combined C5–C6$^\gamma$ interaction, featuring two types of H-bond concurrently, enhanced by hyper-conjugation effects and leading to well-defined low-energy conformer shapes in gas and solution phases (Fig. 1).

Methods

Attc was prepared by an adaptation of the literature method[41] and its derivatives 1–3, each capped at the N-terminal with a benzylcarbamate group (Cbz-cap) and at the C-terminal as a methylamide, were prepared using standard solution phase procedures (see ESI Section 1 for syntheses†) (Fig. 2). Standard IR and NMR spectroscopic methods were used to perform solution state conformational analysis using dilute sample solutions in a low polarity solvent (chloroform) and solid state analysis using single crystal X-ray diffraction. Details are provided in the ESI document.†

Experimental characterization focused on gas phase spectroscopy because in these conditions vibrationally resolved spectra can be obtained for systems composed of several residues, providing that care is taken to use a soft vaporisation technique along with an efficient rotational and vibrational cooling. This was achieved by combining a laser desorption set-up, bringing intact molecules into the gas phase, with the adiabatic expansion of a molecular jet.[42] Furthermore using the sophisticated arsenal of gas phase laser techniques, which combines both UV and IR spectroscopy, namely the so-called IR/UV double resonance laser spectroscopy, conformational selectivity can be achieved.[42] Using this strategy, conformer-specific IR spectra of each isolated compound 1–3 were obtained.

Comparison of the vibrationally resolved spectra with the theoretical IR spectra of low energy conformations allowed assignment of the observed conformers to specific conformations and thereby provided a detailed description of the intra-molecular H-bond network of each conformation. The theoretical IR spectra were obtained by a three-step strategy combining several theoretical chemistry methods (see ESI Section 3†). First, exploration of the potential energy landscape of each compound was performed combining the OPLS-2005 force field with the Monte-Carlo multiple minima method.[43] Second, geometry of the conformations selected during the exploration step was then optimized using the DFT-D quantum chemistry method (RI-B97-D3(BJ)-abc/def2-TZVPPD level).[44–46] Finally, at the same level of theory, a frequency calculation was performed within the harmonic approximation for each optimized geometry. These calculations verified that the conformations corresponded to "true" minima and the harmonic frequencies derived were rescaled using scaling factors in order to generate theoretical IR spectra. In addition, detailed NBO analyses[47–50] were performed for each conformation, leading to quantitative information on the strength of the intramolecular

H-bonds as well as on hyperconjugation effects. These experimental and computational techniques have been described previously[51–53] (details are given in ESI Sections 2 and 3†).

The Cbz-cap, which provides the UV chromophore required for the IR/UV double resonance spectroscopy, gives rise to rotamers (a phenomenon that we refer to as Cbz-rotamerism) which share essentially the same amide backbone and hence very similar, although distinct, IR spectra. Narrow UV spectral signatures were observed in the origin region of the first $\pi\pi^*$ transition of the phenyl group (Fig. 3a), reflecting the rotational and vibrational cooling provided by the jet. Each was used in IR/UV double resonance spectroscopy to acquire conformer-selective IR spectra (see ESI Section 4.5†), whose analysis showed that the doublet bands, labelled A and A_1, in compounds **1** and **2**, were respectively consistent with origins and less intense vibronic bands (involving a low frequency torsional mode of the Cbz-cap) of the same Cbz-cap rotamer.

This illustrated the efficient conformational cooling achieved in the supersonic expansion, which funnels the rotamer population into the most stable species. In the UV spectrum of compound **2**, the red-shifted isolated band, labelled B, suggested a different interaction between the amide backbone and the side chain. Intriguingly, in **3**, the complex feature observed nearly coincides with the doublets observed for compounds **1** and **2**, with a splitting of the intense band into two components labelled A and A′.

The conformer-specific IR spectra collected from the several band systems (A, A′ and B) were assigned to the most stable conformations, obtained from the exploration of the potential energy landscape (see ESI Sections 4.1–4.3†) for which a best agreement was met between experimental and theoretical IR spectra, usually with discrepancies not larger than 20 cm⁻¹ for each NH stretch band,[52] and generally with an accuracy of 30 cm⁻¹ in the case of N–H···S H-bonds.[31] (see ESI Section 4 for complete sets of spectra.†)

Results and discussion

Conformer-specific NH stretch IR spectra of compound **1** revealed the presence of only one conformer family (ESI Section 4.1†), characterized by two strong vibrational bands at 3360 and 3398 cm⁻¹, implicating two distinct H-bonds simultaneously
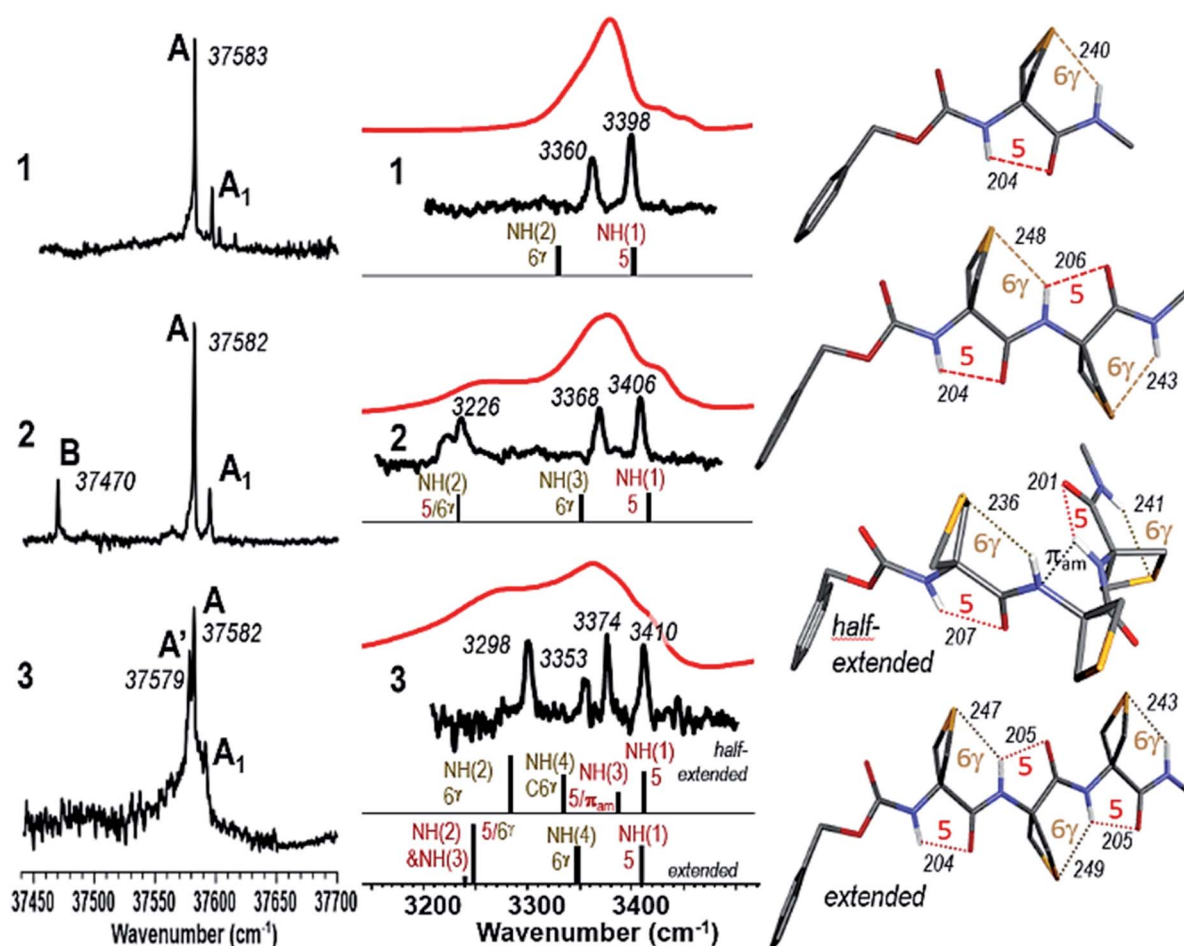

Fig. 3 (left) Gas phase UV spectra of jet-cooled compounds **1–3**. (centre) Gas phase IR spectra (black), obtained on UV bands A (**1** and **2**) or A′ (**3**), and solution phase spectra (red) of compounds **1–3**, compared to the theoretical IR spectrum (stick) of the Cbz-cap *trans* rotamer of the lowest energy conformations. (right) Corresponding calculated lowest energy conformations of **1**, **2**, **3** (half-extended conformer) and **3** (extended conformer).

(Fig. 3). Comparison with the most stable calculated conformations (see Table S2, Fig. S2 and S3†) enabled their respective assignments to a 6-membered ring N–H⋯S H-bond (designated C6$^\gamma$, where the superscript refers to the γ-position occupied by the S atom in the side chain) implicating NH(2) and an intra-residue C5 N–H⋯O=C interaction implicating NH(1), which together constitute a C5–C6$^\gamma$ structural feature characterized by an extended planar backbone (Fig. 3). The strengths of these H-bonds, as judged by the calculated H-bond interatomic distances (Table 1), were comparable with those observed in species where only one such interaction exists – the C5 form of Ac-Aib-NHMe[53] and in the N–H⋯S intermolecular H-bond of the N-methylacetamide·SMe$_2$ complex (see Fig. S4†) – suggesting the mutual compatibility of these interactions. NBO analysis of the stabilization energies induced by the H-bonding (Tables 1 and S5†) confirmed the unusual stabilization of the extended planar backbone (C5 H-bond) and emphasized the role of hyperconjugation effects between each of the C$^\alpha$–C$^\beta$ bonds and vicinal covalent bonds or sites of the backbone, in particular that originating from the lone pair of N(1) which provides a stabilisation energy in the 40 kJ mol^{-1} range (see details in ESI section 4.4†).

Conformer-specific NH stretch IR spectra of compound 2 revealed the presence of two conformer families (ESI Section 4.2†). The major family was assigned to the most stable calculated conformation (Fig. 3) which displayed an extended planar backbone composed of two successive C5–C6$^\gamma$ monomer motifs (designated C5–C6$^\gamma$/C5–C6$^\gamma$). This structure gives rise to two H-bonds in the same spectral range implicating NH(1) in a C5 interaction and NH(3) in a C6$^\gamma$ interaction, and a third which was considerably more red-shifted (at 3226 cm^{-1}) implicating NH(2) which was engaged simultaneously in two contiguous C5–C6$^\gamma$ structures (Fig. 3). The bond distances (Table 1) showed significant elongation of the C6$^\gamma$ bonds, especially that involving NH(2), signalling some frustration. Nonetheless, in this conformation NH(2) was engaged in a three-centre H-bond of the type C=O⋯H(N)⋯SR$_2$, an H-bonding pattern which, as far as we are aware, is without precedent. NBO analysis of the significant stabilization energies (Tables 1 and S5†) confirmed

the juxtaposition of two successive C5–C6$^\gamma$ monomer motifs, slightly weakened compared to 1 (see details in ESI Section 4.4†) and connected by a three-centre H-bond, with NH(2) as the double donor. The minor family, accounting for about 16% of the vaporized sample (B band in the UV spectrum of Fig. 3a), had a backbone which showed two successive γ-turns (Fig. S5 and S6†). It was found to be favoured by a dispersive contact between a Cbz-cap, in a gauche rotamer, and the C-terminus end of the backbone.

Conformer-specific NH stretch IR spectra of compound 3 revealed the presence of a single backbone family (ESI Section 4.3†), characterized by four H-bonds of various strengths spanning a spectral range of 120 cm^{-1} (Fig. 3). The theoretical conformational landscape (Fig. S7†) suggested that two nearly isoenergetic ($\Delta G = 2.2$ kJ mol^{-1}) low energy conformation families might exist, namely a half-extended (i.e. partly folded) conformer featuring two C5–C6$^\gamma$ motifs separated by a Ramachandran α-type backbone configuration (a local feature with a double donor role for NH(3), designated C5-π_{am}, which has been observed only once before, in a stable conformation of a capped Aib dipeptide[54]), and an extended, planar C5–C6$^\gamma$/C5–C6$^\gamma$/C5–C6$^\gamma$ structure, perceived as a propagation of the structure adopted by 2. Comparison of experimental and theoretical IR spectra (Fig. 3) revealed that 3 adopts the half-extended structure, whose non-planar backbone furthermore accounts for the splitting of the UV features (A and A′ bands) due to a degeneracy lifting between gauche$^+$ and gauche$^-$ Cbz-cap rotamers (see ESI Section 4.5†). The elongated N–H⋯S distances in the extended form of 3 compared to that in 1 (by 3–9 pm) suggested increased frustration in the former. In contrast, the NH(2)⋯S(1) distance in the half-extended form of 3 was shorter (by 4 pm) and the H-bond appeared commensurately stronger (by 11 kJ mol^{-1}) than in 1 (Table 1). NBO analysis of the significant stabilization energies (Tables 1 and S5†) showed that the "missing" H-bond in the half-extended conformer was compensated by (i) an enhancement of the two remaining C6$^\gamma$ interactions, (ii) by specific hyperconjugation interactions from the thietane rings to the backbone, in particular those vicinal interactions not involving sulphur (see

Table 1 H-bond distances, Ramachandran dihedral angles and stabilization energies ($E^{(2)}$) associated with H-bonds, as obtained from the NBO analysis. All data from this work unless otherwise indicated. (For full details of NBO analysis, in particular hyperconjugative interactions see ESI Section 4.4.)

Compound	Residue	Distance NH(i)⋯O (pm)	Distance NH($i + 1$)⋯S (pm)	Distance NH(i)⋯π_{am}(i) (pm)	ϕ (°)	ψ (°)	$E^{(2)}$ C5 (kJ mol^{-1})	$E^{(2)}$ C6$^\gamma$ (kJ mol^{-1})	$E^{(2)}$ π_{am} (kJ mol^{-1})
Ac-Aib-NHMe (C5)[53]		204			180	179	14.6		
AcNHMe·SMe$_2$			247					35.6	
1	1	204	240		180	180	13.9	32.3	
2	1	204	248		179	180	13.0	26.9	
	2	206	243		180	180	19.1	29.2	
3 half-extended	1	207	236	—	180	179	11.4	42.7	—
	2	—	—	230	65	29	—	—	3.1
	3	201	241	—	174	177	18.6	31.6	—
3 extended	1	204	247		180	180	13.4	27.8	
	2	205	249		180	180	17.7	24.8	
	3	205	243		180	180	19.1	28.6	

Table S5,† interactions HC$^\alpha$ and HC$^\beta$) and (iii) more marginally by a weak interaction of NH(3) with the π system that implicates N(2) (see details in ESI Section 4.4†).

We looked for evidence for the C5–C6$^\gamma$ structural features in solution phase using IR and NMR spectroscopic techniques. The IR absorption spectra of compounds 1–3 were recorded in chloroform solution (5 mM) and showed no significant changes upon 10-fold dilution, pointing to the intramolecular nature of any non-covalent interactions contributing to the main spectral features. In all cases broad amide NH stretch bands were in evidence and, notwithstanding the lower spectral resolution, good overall correlation was observed with gas phase experimental and theoretical spectra for the lowest-energy conformations (Fig. 3). The IR spectrum of compound 1 showed one broad band centred at around 3375 cm^{-1} which we assigned to the overlap of NH(1) in a medium strength C5 interaction and NH(2) implicated in a C6$^\gamma$ feature. In compound 2 the NH(3) C6$^\gamma$ vibration remained at around 3370 cm^{-1} and the red-shifted NH(2) now appeared as a plateau at around 3250 cm^{-1}. The appearance of a shoulder at 3410 cm^{-1} was attributed to an attenuated C5 interaction of NH(1). For compound 3 the IR spectrum was consistent with a weak C5 vibration for NH(1) at 3410 cm^{-1}, C6$^\gamma$ features for NH(2) and NH(4), and some type of H-bonding for NH(3); these data were in good agreement with the half-extended conformation although they did not formally exclude the extended form. For comparison purposes, the derivative Cbz-Attc-OMe 4 was prepared and its IR spectrum recorded in chloroform (see ESI Sections 1.2 and 5.1†). With a now weaker H-bond acceptor than that in 1 (an ester instead of an amide), the main absorption band at 3440 cm^{-1} was assigned to a free NH vibration while a minor band at 3410 cm^{-1} indicated a contribution from a weak C5 H-bonded conformation. The absence of strong absorbance bands for free NH vibrations above 3420 cm^{-1} for compounds 1–3 suggested that conformations having no intramolecular H-bonds are not present. Likewise, conformations implicating larger-ring interactions, such as a C7 structure in 2 or C7 or C10 structures in 3, are of little or no significance, since these would be require at least one free NH group. Collectively, the IR data indicated that the C5–C6$^\gamma$ conformational feature was present for compounds 1–3 in solution, albeit with a weakened C5 interaction at the N-terminal in 2 and 3.

Further support was forthcoming from ^{1}H NMR experiments on compounds 1–3 in solution in CDCl$_3$ (5 mM) (ESI Section 5.2†). All signals were assigned using standard 1D and 2D pulse sequences and were well defined, suggesting the presence of one predominant conformation for each compound. In the spectrum of compound 1 both the carbamate NH(1) signal (δ = 6.45 ppm) and the amide NH(2) signal (δ = 7.98 ppm) were deshielded, suggesting their implication in H-bonds. Titration with DMSO-d_6 induced a non-negligible downfield shift ($\Delta\delta$ = 0.60 ppm for 10% added DMSO) for NH(1), compatible with its involvement in a moderate strength C5 H-bond, while the upfield shift observed for NH(2) ($\Delta\delta$ = −0.68 ppm) suggested no solvent exposure, commensurate with it being H-bonded to sulfur. These data are in full agreement with the proposed C5–C6$^\gamma$ conformer for 1 (Fig. 1). In comparison, titration of a CDCl$_3$

solution of ester 4 with DMSO-d_6 induced a greater downfield shift of the NH signal ($\Delta\delta$ = 1.79 ppm for 10% added DMSO), pointing to extensive solvent exposure. In compound 2 the carbamate NH(1) was more shielded (δ = 6.23 ppm) than in 1. Amide NH(3) was deshielded (δ = 7.84 ppm) while amide NH(2) was strongly deshielded (δ = 8.95 ppm), this latter corresponding to a 3-centre H-bonded system. Titration with DMSO-d_6 induced a considerable downfield shift ($\Delta\delta$ = 1.38 ppm) for NH(1), confirming the weakness of its C5 H-bond, while upfield shifts were observed for NH(2) and NH(3) ($\Delta\delta$ = −0.79 and −0.99 ppm respectively). Data for compound 3 were more difficult to interpret unequivocally but were fully compatible with the adoption of the combined C5–C6$^\gamma$ structural features suggested above. The carbamate NH(1) signal (δ = 6.26 ppm) was comparable to that of 2, while NH(4) was deshielded (δ = 7.52 ppm) and NH(2) and NH(3) were strongly deshielded (δ = 8.32 and 8.39 ppm). Titration with DMSO-d_6 induced a downfield shift ($\Delta\delta$ = 1.89 ppm) for the weakly C5 H-bonded NH(1) and small downfield (or upfield) shifts for NH(2), NH(3) and NH(4) ($\Delta\delta$ = 0.30, −0.94 and −0.89 ppm, respectively).

A NOESY experiment carried out on compound 2 (ESI Section 5.3†) provided a correlation map that was in complete agreement with the C5–C6$^\gamma$/C5–C6$^\gamma$ conformation. Medium cross peaks were observed between NH(i) and both C$^\beta$H(a) protons for each Attc(i) and strong cross peaks were observed between NH(i + 1) and both C$^\beta$H(b) protons for each Attc(i) (Fig. 4).

Compounds 1–3 were solids and for completeness we conducted X-ray diffraction analysis on single crystals. The C5–C6$^\gamma$ feature was not present in the crystal lattices; instead, strong intermolecular H-bonding networks were in evidence in all three cases (ESI Section 6†). The molecular structures of the three compounds are shown in Fig. 5. Compound 1 showed only
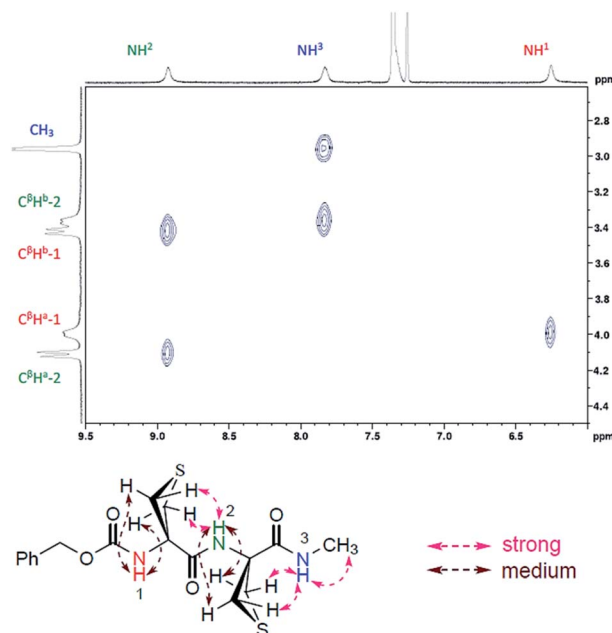

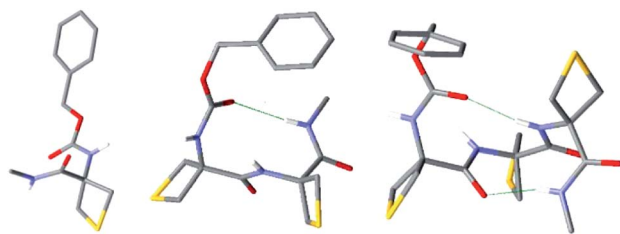Fig. 4 Significant NOESY correlations observed for compound 2 and their assignments.

Fig. 5 X-ray crystal structures of **1–3** (left to right). Only one of the three molecules in the unit cell is shown for **2**. Intramolecular C10 H-bonding interactions are shown for **2** and **3**. Only NH hydrogen atoms are shown for clarity.

intermolecular N–H⋯O=C interactions in the lattice, implicating both NH and both carbonyl groups of each molecule. For compound **2** the asymmetric unit contained three molecules, each of which displayed an intramolecular C10 H-bonding interaction between NH(3) and the Cbz-cap C=O, with N–H⋯O=C distances of 219, 233 and 230 pm in the three distinct molecules. The crystal structure of compound **3** showed a conformation with two consecutive C10 interactions, which constituted a short 3_{10}-helix. NH(3) and NH(4) interacted with the Cbz-cap C=O and the carbonyl of Attc(1), respectively, with N–H⋯O=C distances of 208 and 218 pm, respectively. In all three crystal structures, the closest contacts for the sulfur atoms were with aromatic hydrogen atoms on the Cbz-cap phenyl rings of neighbouring molecules in the lattices, with H⋯S distances in the range 280–295 pm (ESI Section 6†). Such interactions, in which a thioether sulfur atom is located near the edge and slightly above the plane of the aromatic ring, have been observed before in crystal structures of proteins[55] and of small molecules.[56] The conformations adopted by **1–3** in the solid state are incompatible with the solution phase and gas phase data presented and discussed above.

Conclusion

In summary, the unique properties of the thietane ring of Attc derivatives lead to the adoption of hyperconjugation-assisted C5–C6$^\gamma$ locally-planar structures in the gas phase and in solution phase, providing a new axiom for H-bonding. This discovery may facilitate the development of new tools for contributing to conformation control in small peptides, *e.g.* in the stabilization of extended backbone geometries[57] or for the design of new peptidomimetic or foldamer architectures in a non-polar environment, and should provide a stimulus for further reflections on the significance of the less conventional N–H⋯S H-bond.

Conflicts of interest

There are no conflicts to declare.

Acknowledgements

Notes and references

1 G. Gilli and P. Gilli, *The Nature of the Hydrogen Bond. Outline of a Comprehensive Hydrogen Bond Theory*, Oxford University Press, New-York, USA, 2009.

2 P. M. Pihko, *Hydrogen Bonding in Organic Synthesis*, Wiley-VCH, Weinhein, Germany, 2009.

3 A. D. Burrows, in *Supramolecular Assembly Via Hydrogen Bonds I*, ed. D. M. P. Mingos, 2004, vol. 108, pp. 55–95.

4 D. Braga, L. Maini, M. Polito and F. Grepioni, in *Supramolecular Assembly Via Hydrogen Bonds II*, ed. D. M. P. Mingos, 2004, vol. 111, pp. 1–32.

5 S. Hecht and I. Huc, *Foldamers: Structure, Properties, and Applications*, Wiley-VCH, Weinheim, Germany, 2007.

6 Y. Lan, M. G. Corradini, R. G. Weiss, S. R. Raghavan and M. A. Rogers, *Chem. Soc. Rev.*, 2015, **44**, 6035–6058.

7 G. R. Desiraju and T. Steiner, *The Weak Hydrogen Bond in Structural Chemistry and Biology*, Oxford University Press, New York, USA, 1999.

8 C. L. Perrin and J. B. Nielson, *Annu. Rev. Phys. Chem.*, 1997, **48**, 511–544.

9 G. A. Jeffrey and W. Sänger, *Hydrogen Bonding in Biological Structures*, Springer-Verlag, Berlin, Germany, 1991.

10 A. Karshikoff, *Non-covalent Interactions in Proteins*, Imperial College Press, London, UK, 2006.

11 E. N. Baker and R. E. Hubbard, *Prog. Biophys. Mol. Biol.*, 1984, **44**, 97–179.

12 G. D. Rose, L. M. Gierasch and J. A. Smith, *Adv. Protein Chem.*, 1985, **37**, 1–109.

13 C. Peggion, A. Moretto, F. Formaggio, M. Crisma and C. Toniolo, *Biopolymers*, 2013, **100**, 621–636.

14 R. W. Newberry and R. T. Raines, *Nat. Chem. Biol.*, 2016, **12**, 1084.

15 M. Crisma, F. Formaggio, C. Aleman, J. Torras, C. Ramakrishnan, N. Kalmankar, P. Balaram and C. Toniolo, *Pept. Sci.*, 2018, **110**, e23100.

16 Z. S. Derewenda, L. Lee and U. Derewenda, *J. Mol. Biol.*, 1995, **252**, 248–262.

17 S. Horowitz and R. C. Trievel, *J. Biol. Chem.*, 2012, **287**, 41576–41582.

18 G. J. Bartlett, A. Choudhary, R. T. Raines and D. N. Woolfson, *Nat. Chem. Biol.*, 2010, **6**, 615–620.

19 V. R. Mundlapati, D. K. Sahoo, S. Bhaumik, S. Jena, A. Chandrakar and H. S. Biswal, *Angew. Chem., Int. Ed.*, 2018, **57**, 16496–16500.

20 D. A. Dougherty, *Science*, 1996, **271**, 163–168.

21 T. W. Craven, M. K. Cho, N. J. Traaseth, R. Bonneau and K. Kirshenbaum, *J. Am. Chem. Soc.*, 2016, **138**, 1543–1550.

22 R. W. Newberry and R. T. Raines, *ACS Chem. Biol.*, 2019, **14**, 1677–1686.

23 C. C. Valley, A. Cembran, J. D. Perlmutter, A. K. Lewis, N. P. Labello, J. Gao and J. N. Sachs, *J. Biol. Chem.*, 2012, **287**, 34979–34991.

24 E. A. Meyer, R. K. Castellano and F. Diederich, *Angew. Chem., Int. Ed.*, 2003, **42**, 1210–1250.

25 M. Iwaoka, S. Takemoto, M. Okada and S. Tomoda, *Bull. Chem. Soc. Jpn.*, 2002, **75**, 1611–1625.

26 F. Formaggio, M. Crisma, C. Toniolo and C. Peggion, *Eur. J. Org. Chem.*, 2013, 3455–3463.

27 V. R. Mundlapati, S. Gautam, D. K. Sahoo, A. Ghosh and H. S. Biswal, *J. Phys. Chem. Lett.*, 2017, **8**, 4573–4579.

28 L. M. Gregoret, S. D. Rader, R. J. Fletterick and F. E. Cohen, *Proteins*, 1991, **9**, 99–107.

29 P. Zhou, F. F. Tian, F. L. Lv and Z. C. Shang, *Proteins*, 2009, **76**, 151–163.

30 H. S. Biswal, E. Gloaguen, Y. Loquais, B. Tardivel and M. Mons, *J. Phys. Chem. Lett.*, 2012, **3**, 755–759.

31 V. R. Mundlapati, S. Ghosh, A. Bhattacherjee, P. Tiwari and H. S. Biswal, *J. Phys. Chem. Lett.*, 2015, **6**, 1385–1389.

32 B. Yan, S. Jaeqx, W. J. van der Zande and A. M. Rijs, *Phys. Chem. Chem. Phys.*, 2014, **16**, 10770–10778.

33 M. Alauddin, H. S. Biswal, E. Gloaguen and M. Mons, *Phys. Chem. Chem. Phys.*, 2015, **17**, 2169–2178.

34 H. Tang, R. J. Doerksen, T. V. Jones, M. L. Klein and G. N. Tew, *Chem. Biol.*, 2006, **13**, 427–435.

35 P. Du, X. K. Jiang and Z. T. Li, *Tetrahedron Lett.*, 2009, **50**, 320–324.

36 M. Palumbo, S. Darin, G. M. Bonora and C. Toniolo, *Macromol. Chem. Phys.*, 1976, **177**, 1477–1492.

37 C. Toniolo, G. M. Borona and A. Scatturin, *Gazz. Chim. Ital.*, 1975, **105**, 1063–1071.

38 A. A. Ribeiro, M. Goodman and F. Naider, *Int. J. Pept. Protein Res.*, 1979, **14**, 414–436.

39 M. De Zotti and J. Clayden, *Org. Lett.*, 2019, **21**, 2209–2212.

40 I. Torrini, G. P. Zecchini, M. P. Paradisi, G. Lucente, G. Mastropietro, E. Gavuzzo, F. Mazza, G. Pochetti, S. Traniello and S. Spisani, *Biopolymers*, 1996, **39**, 327–337.

41 A. P. Kozikowski and A. H. Fauq, *Synlett*, 1991, 783–784.

42 E. Gloaguen and M. Mons, *Top. Curr. Chem.*, 2015, **364**, 225–270.

43 *Macromodel Schrödinger*, LLC, New York, NY, USA, Schrödinger Release 2019-3, and references therein.

44 S. Grimme, J. Antony, S. Ehrlich and H. Krieg, *J. Chem. Phys.*, 2010, **132**, 154104.

45 D. Rappoport and F. Furche, *J. Chem. Phys.*, 2010, **133**, 134105.

46 K. Eichkorn, F. Weigend, O. Treutler and R. Ahlrichs, *Theor. Chem. Acc.*, 1997, **97**, 119–124.

47 A. E. Reed, L. A. Curtiss and F. Weinhold, *Chem. Rev.*, 1988, **88**, 899–926.

48 F. Weinhold, *J. Comput. Chem.*, 2012, **33**, 2363–2379.

49 I. V. Alabugin, G. dos Passos Gomes and M. A. Abdo, *Wiley Interdiscip. Rev.: Comput. Mol. Sci.*, 2019, **9**, e1389.

50 I. V. Alabugin, K. M. Gilmore and P. W. Peterson, *Wiley Interdiscip. Rev.: Comput. Mol. Sci.*, 2011, **1**, 109–141.

51 E. Gloaguen, H. Valdes, F. Pagliarulo, R. Pollet, B. Tardivel, P. Hobza, F. Piuzzi and M. Mons, *J. Phys. Chem. A*, 2010, **114**, 2973–2982.

52 E. Gloaguen and M. Mons, *Top. Curr. Chem.*, 2015, **364**, 225–270.

53 V. Brenner, E. Gloaguen and M. Mons, *Phys. Chem. Chem. Phys.*, 2019, **21**, 24601–24619.

54 J. R. Gord, D. M. Hewett, A. O. Hernandez-Castillo, K. N. Blodgett, M. C. Rotondaro, A. Varuolo, M. A. Kubasik and T. S. Zwier, *Phys. Chem. Chem. Phys.*, 2016, **18**, 25512–25527.

55 K. S. C. Reid, P. F. Lindley and J. M. Thornton, *FEBS Lett.*, 1985, **190**, 209–213.

56 R. J. Zauhar, C. L. Colbert, R. S. Morgan and W. J. Welsh, *Biopolymers*, 2000, **53**, 233–248.

57 C. Toniolo, M. Crisma, F. Formaggio and C. Peggion, *Biopolymers*, 2001, **60**, 396–419.